Statistical design of experiments for evaluation of Y–Zr–Ti oxides as anode materials in solid oxide fuel cells

F. Tietz, I. Arul Raj and D. Stöver

Mixed conducting anode materials for solid oxide fuel cells are desirable in order to extend the electron transfer reaction zone for fuel gas conversion and to minimise the nickel content for achieving a redox stable anode. Partial substitution by titania in yttria stabilised zirconia (YSZ) is known to increase the electronic conductivity in reducing atmospheres. Nine different compositions were selected from the quasi ternary phase diagram according to principles used in statistical design of experiments covering the whole stoichiometric regime relevant for ionic applications. The dc electrical conductivity values increase strongly with high Ti contents under reducing (Ar–4%H_2) conditions, whereas they decrease continuously with increasing Ti content under oxidising conditions (air). The results clearly show that the chosen screening process for materials selection can considerably reduce the number of samples. For solid oxide fuel cell anodes, the compositions in the $YO_{1.5}$–ZrO_2–TiO_2 system should be restricted to low Ti contents. BCT/0426

Keywords: Electrical properties, Fuel cells, Statistical design of experiments, $YO_{1.5}$–ZrO_2–TiO_2 phase diagram.

The authors are at Forschungszentrum Jülich GmbH, Institute for Materials and Processes in Energy Systems (WV-1), D–52425 Jülich, Germany (f.tietz@fz-juelich.de); Dr Arul Raj is on leave from the Central Electrochemical Research Institute (CECRI), Karaikudi 630 006, Tamil Nadu, India.
Manuscript received 5 April 2004; accepted in revised form 27 July 2004.

INTRODUCTION

Alternative functional materials for the operation of solid oxide fuel cells (SOFCs) in the temperature range 650–800°C have been investigated by several research groups in recent years.[1–11] The focus of this international effort lies very much on the improvement of several critical functional characteristics of the ceramic components and their performance endurance within the cell. Several new fast oxide ion conducting solid electrolytes,[3,4,12–14] cathode materials,[1,10,11,15–17] contact layer materials for the cathode/steel interface[18–20] and new composite anode materials[21–27] have been investigated for this purpose.

The requirements posed by an efficient SOFC anode material are many and hence the search for alternative materials is complex. State of the art Ni/YSZ anodes are less expensive and Ni is known to exhibit high catalytic activity for the anodic hydrogen oxidation reaction. Hence this anode material is widely used in SOFCs with hydrogen as fuel. The loading of Ni is chosen to be around 40 vol.-% of solids in order to promote the percolation electronic conduction in the bulk anode substrate. However, higher Ni loading brings in thermal mismatch between the Ni/YSZ anode and the 8 mol-% yttria stabilised zirconia (8YSZ) electrolyte. Moreover, if the anode fuel does not contain sufficient amounts of steam, Ni in the anode acts as a catalyst to promote competitive catalytic cracking of hydrocarbons. The deposition of carbon onto the Ni/YSZ cermet anode demonstrates that direct electrochemical oxidation of dry methane is not technically feasible in SOFCs.[28,29] Therefore several ceramic materials have been investigated as anode materials but without significant success, because the pure ceramics did not act as catalysts.[30–32] Just recently a study has demonstrated ceramic anodes based on $(La,Sr)TiO_3$/$(Ce,La)O_2$ composites with remarkably low overpotentials, which might be applicable in SOFCs in the future.[33]

As in $(La,Sr)TiO_3$ materials,[32–35] electronic conductivity in the Y–Zr–Ti–O (YZT) system arises from the partial reduction of Ti^{4+} ions to Ti^{3+}.[36] Although about two dozen papers on YZT ceramics are available, little has been published on the systematic dependence of electrical properties on stoichiometry.[24,25,37–41] Only the work of Colomer *et al.*[40,41] resulted in a mapping of conductivities by extended variation of Y and Ti contents. An attempt was therefore made in the present study to characterise the relevant stoichiometric region in the $YO_{1.5}$–ZrO_2–TiO_2 phase diagram by means of statistical design of experiments using only nine different powder compositions and to prove this method as a tool for sophisticated but rapid materials selection.

EXPERIMENTAL PROCEDURES

Materials selection

In the YZT system the most relevant compositions for ionic applications range from about 8 to 20 at.-%$YO_{1.5}$ for achieving high ionic conductivity and from 0 to about 20 at.-%TiO_2 to stay within the single phase region of the cubic fluorite structure.[41,42] To avoid the preparation of several solid solutions with multiple compositions, a statistical design of experiments approach was used, the so called 'central composite design'. In this design only nine different compositions were chosen by variation of the yttria and titania contents as shown in Table 1 and Fig. 1. Typically such designs give results with high statistical confidence.[43–45] It was therefore expected that these nine compositions would constitute a true representation of all available compositions arising out of the chosen regime of the phase diagram. Table 1 also shows how the compositions, i. e. the Y and Ti contents, are transferred to orthogonal coordinates for subsequent statistical evaluation.

DOI 10.1179/096797804X4213

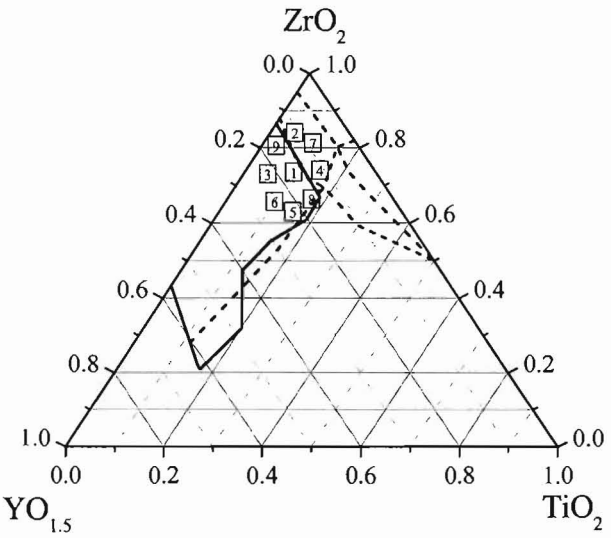

1 Part of ternary phase diagram showing region of single phase cubic fluorite (solid line)[42] and Zr rich phase regions (dashed lines) as determined in Ref. 41: position of nine YZT powders indicated by numbered squares

Powder synthesis

Powders with the planned nominal composition were prepared by a coprecipitation technique as reported previously.[36] The respective nitrate salts of Zr and Y for the preparation of 50 g of each powder were weighed and dissolved in double distilled water to produce a clear solution. The necessary quantity of hydrochloric aqueous $TiCl_3$ containing solution (1 mL of $TiCl_3$ solution contained 57·5 mg of Ti) was added in drops to this clear solution with continuous stirring. Brisk effervescence and yellowish fumes of nitrogen oxides appeared during stirring owing to the oxidation of Ti^{3+} ions. The whole mixture was stirred for 1 h to ensure homogeneity. An aqueous ammonia solution was slowly added to the solution with continuous stirring in order to precipitate all metal cations as hydroxides. The pH of the contents was maintained at 9·5. The precipitate was stirred for 1 h and then allowed to settle. After filtration and washing until the precipitate was completely free from chloride ions, it was subsequently dried overnight in an air oven at 110°C. The remaining solid was crushed well in an agate mortar and the powder was subjected to calcination at 700°C for 5 h in air, resulting in weight loss of 10–15·5%. Finally, the powders were ball milled using zirconia balls for 24 h.

The calcined powders were chemically analysed by inductively coupled atomic emission spectroscopy under argon plasma (ICP–OES) to ascertain whether the observed elemental composition of the oxides was consistent with the nominal elemental composition.

Sample preparation

To prepare circular pellets (8 mm diameter) and rectangular bars (40 mm length, 4 mm width, 5 mm height) from the powders, one to two drops of 2% solution of polyvinyl alcohol dissolved in distilled water were added as binder to about 0·6 or 2·0 g of powder, respectively. The homogeneous mixture of the powder and binder was uniaxially pressed at 300 MPa to produce circular pellets and 400 MPa for rectangular bars. The circular pellets were subjected to various programmed sintering conditions with a view to investigating their volume shrinkage and to determining densification behaviour as a function of sintering temperature in air. The sintering procedure involved heating at a rate of 180 K h^{-1} to final temperature, 5 h dwell time and normal cooling to room temperature. The final temperatures used were 1300, 1400 and 1500°C. A second set of pellets was also sintered at 1300°C for 36 h. The resulting changes in the geometrical dimensions of the pellets were measured before and after sintering. The rectangular bars fabricated from the powders were sintered at 1500°C for 5 h in air.

For X-ray diffraction (XRD), parts of the circular pellets sintered at 1300°C for 36 h and the rectangular bars sintered at 1500°C for 5 h were crushed into powder. The two sintering temperatures are representative for investigating the evolution of crystalline phases in the selected compositions as a function of temperature.[36] The experiments were performed at room temperature using a Siemens D5000 diffractometer and Cu K_α radiation.

DC electrical conductivity and microstructural characterisation

For four probe dc conductivity measurements, four silver wires were wrapped around the sintered rectangular bars at symmetrically equal distances from the ends. Intimate contact was realised by using conducting silver paste (Demetron Leitsilber 200). In order to resolve electronic and ionic contributions of the total electrical conductivity, the first temperature dependent measurement between 300 and 900°C was carried out in air, giving the ionic conductivity of the material. A second measurement was carried out in Ar–4%H_2 after equilibrating the samples at 900°C for 24 h. DC measurements do not give a deep fundamental understanding of the system under investigation, but they nevertheless help to evaluate it. A fundamental study was beyond the scope of the present work, and therefore no impedance spectroscopy or more sophisticated methods such as Hebb–Wagner polarisation measurements were carried out to distinguish more precisely between ionic and electronic conductivity.

After the conductivity measurements, the rectangular bars were cut at one edge and the cross-sectional surfaces were then polished in order to investigate sample microstructure. Microstructural parameters such as porosity, average grain size and pore size distribution were used to

Table 1 Nominal powder compositions and orthogonalised coordinates resulting in central composite design: $x_Y=(c_Y-0{\cdot}165)/0{\cdot}055$, $x_{Ti}=(c_{Ti}-0{\cdot}1)/0{\cdot}05$

No.	Nominal composition	Y content c_Y, at.-%	Ti content c_{Ti}, at.-%	x_Y	x_{Ti}
1	$Y_{0{\cdot}165}Zr_{0{\cdot}735}Ti_{0{\cdot}1}O_{2-x}$	0·165	0·10	0	0
2	$Y_{0{\cdot}11}Zr_{0{\cdot}84}Ti_{0{\cdot}05}O_{2-x}$	0·11	0·05	−1	−1
3	$Y_{0{\cdot}22}Zr_{0{\cdot}73}Ti_{0{\cdot}05}O_{2-x}$	0·22	0·05	1	−1
4	$Y_{0{\cdot}11}Zr_{0{\cdot}74}Ti_{0{\cdot}15}O_{2-x}$	0·11	0·15	−1	1
5	$Y_{0{\cdot}22}Zr_{0{\cdot}63}Ti_{0{\cdot}15}O_{2-x}$	0·22	0·15	1	1
6	$Y_{0{\cdot}243}Zr_{0{\cdot}657}Ti_{0{\cdot}1}O_{2-x}$	0·243	0·10	$\sqrt{2}$	0
7	$Y_{0{\cdot}087}Zr_{0{\cdot}813}Ti_{0{\cdot}1}O_{2-x}$	0·087	0·10	$-\sqrt{2}$	0
8	$Y_{0{\cdot}165}Zr_{0{\cdot}664}Ti_{0{\cdot}171}O_{2-x}$	0·165	0·171	0	$\sqrt{2}$
9	$Y_{0{\cdot}165}Zr_{0{\cdot}806}Ti_{0{\cdot}029}O_{2-x}$	0·165	0·029	0	$-\sqrt{2}$

correct the measured effective conductivity data and to calculate the specific conductivity, applying the formula[46,47]

$$\sigma^0 = \sigma^c[(1-\rho_P/\rho_0)+\rho_P/\rho_0 R]/(\rho_P/\rho_0)^2 R \quad . \quad . \quad . \quad . \quad (1)$$

where σ^0 is the specific and σ^c the effectively measured conductivity of the YZT ceramic, ρ_P the density of the porous material and ρ_0 the density of the pore free matrix, and R either the particle size ratio d_{pore}/d_{YZT} or the ratio of the corresponding intercept lengths l_{pore}/l_{YZT},[47] which are parameters that may be obtained from the microstructural analysis. According to ASTM standard E112–63, particle size (pore diameter) is related to the intercept lengths for equiaxed but irregularly shaped objects by

$$d_i = 1{\cdot}13 l_i \quad . \quad . \quad . \quad . \quad . \quad . \quad . \quad . \quad . \quad . \quad . \quad . \quad . \quad . \quad (2)$$

Digital images of the cross-sections of the densified bars were generated using a microscope (Axiomat, Zeiss) equipped with a high resolution digital camera (Siemens K300) and imaging system (KS400, Kontron Electronics). Average grain size and average pore size values were measured from five different regions of each sample and at least 10 000 objects were counted for each sample to give reliable statistics. With this system an optical resolution of 250 nm was achieved and the images were digitised into pixels with 256 different scales of grey. Further details on the digital processing and quantitative image analysis procedures are described elsewhere.[48]

RESULTS AND DISCUSSION

Chemical analysis and X-ray diffraction

The analytical chemical compositions of the powders are presented in Table 2. In most cases the differences observed between the analytical and nominal compositions (Table 1) are within the limits of the experimental analytical accuracy of 3 wt-% per atomic species. Only the Ti contents of two powders (nos. 2 and 8) showed significant deviations, of 10 and 6·4% respectively, compared to the nominal composition. All powders were pure white in colour after synthesis.

The crystalline phases formed after sintering at 1300 and 1500°C are listed in Table 2. Whereas only the four powders with the highest Y content crystallised in the cubic phase at 1300°C, all powders with >15 at.-%Y were cubically crystallised after sintering at 1500°C (except no. 8, with the highest Ti content of 17%). Powder no. 2, with an intermediate Y content and low Ti content, showed additional small reflections of tetragonal and monoclinic phases, whereas powders nos. 4 (intermediate Y content but high Ti content) and 7 (low Y content and intermediate Ti content) showed significant amounts of tetragonal and monoclinic phase. Finally, powder no. 8 (intermediate Y content and very high Ti content) showed tetragonal and monoclinic reflections after sintering at 1300°C, but only minor peaks of tetragonal structure beside the cubic reflections after sintering at 1500°C. In summary, these results are in good agreement with the experimentally established[41,42] and theoretically predicted[49] phase diagrams, as shown in Fig. 1 by the inserted lines, although powder nos. 2, 4 and 7 should only consist of cubic and tetragonal phase. The appearance of monoclinic phase is due either to the short sintering time (and thus higher inhomogeneity) of the samples compared with the long annealing time for the phase diagram studies,[41,42] or to the slow cooling of the samples in the furnace.

The lattice parameters and relative amounts of observed crystalline phases were determined in order to calculate the theoretical density of each powder. In the case of a phase mixture, a Rietveld analysis of the intensity profiles was performed to determine at least the amount of monoclinic phase. The resulting theoretical densities (Table 1) differed only slightly from the density taking into account only the cubic lattice parameter. The largest deviation of 2·4% was found for powder no. 7, containing the highest amount of monoclinic phase.

Table 2 Analytical powder compositions, crystalline phases observed by XRD after sintering at 1300 and 1500°C, crystallographic data after sintering at 1500°C and resulting theoretical density of YZT oxides

No.	Analytical composition	Crystalline phases after sintering at 1300°C	Crystalline phases after sintering at 1500°C	Lattice parameters after sintering at 1500°C, pm	Phase content, %	Theoretical density, g cm^{-3}
1	$Y_{0{\cdot}163}Zr_{0{\cdot}740}Ti_{0{\cdot}097}O_{2-x}$	c+t	c	a_c=511·8(2)	100 (c)	6·42
2	$Y_{0{\cdot}107}Zr_{0{\cdot}847}Ti_{0{\cdot}045}O_{2-x}$	c+t+m	c+t+m	a_c=512·2(2) a_t=359·2(2), c_t=517·4(4)	81 (c+t)	6·12
				a_m=530·8(7), b_m=517·2(1·4), c_m=515·2(8), β=98·9(1)	19 (m)	
3	$Y_{0{\cdot}218}Zr_{0{\cdot}735}Ti_{0{\cdot}047}O_{2-x}$	c	c	a_c=513·6(2)	100 (c)	6·13
4	$Y_{0{\cdot}109}Zr_{0{\cdot}746}Ti_{0{\cdot}145}O_{2-x}$	c+t+m	c+t+m	a_c=511·3(3) a_t=357·6(2), c_t=519·0(4)	90 (c+t)	6·61
				a_m=531·6(7), b_m=512·6(1·4), c_m=511·7(8), β=98·5(1)	10 (m)	
5	$Y_{0{\cdot}218}Zr_{0{\cdot}635}Ti_{0{\cdot}147}O_{2-x}$	c	c	a_c=511·4(2)	100 (c)	6·60
6	$Y_{0{\cdot}238}Zr_{0{\cdot}666}Ti_{0{\cdot}096}O_{2-x}$	c	c	a_c=512·7(2)	100 (c)	6·34
7	$Y_{0{\cdot}084}Zr_{0{\cdot}819}Ti_{0{\cdot}097}O_{2-x}$	c+t+m	c+t+m	a_c=511·7(2) a_t=358·9(3), c_t=517·1(6)	46 (c+t)	6·31
				a_m=531·5(7), b_m=515·9(1·4), c_m=513(8), β=98·8(1)	54 (m)	
8	$Y_{0{\cdot}165}Zr_{0{\cdot}675}Ti_{0{\cdot}160}O_{2-x}$	c+t+m	c+t	a_c=510·7(2) a_t=357·3(2), c_t=518·4(4)	68 (c) 32 (t)	6·76
9	$Y_{0{\cdot}162}Zr_{0{\cdot}815}Ti_{0{\cdot}024}O_{2-x}$	c	c	a_c=513·1(2)	100 (c)	6·09

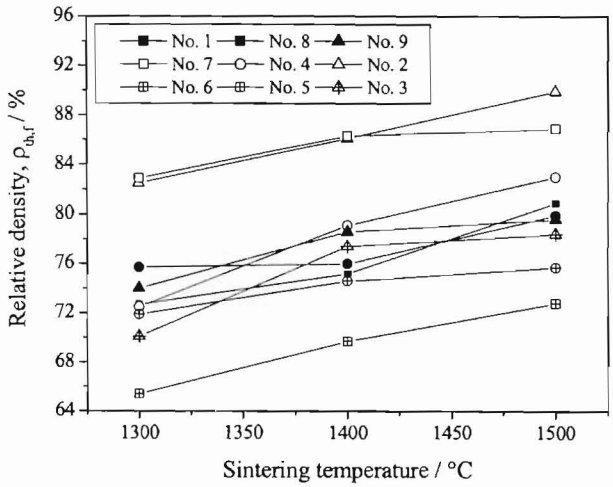

2 Relative densities of circular pellets after sintering with sample symbols grouped according to chemical composition: full, open and crossed symbols correspond to powders with intermediate, low and high Y content respectively; squares, circles and triangles refer to powders with intermediate, high and low Ti content respectively (cf. Fig. 1)

Sintering behaviour and microstructural investigations

In Table 3 the density values of the circular pellets after sintering at 1300–1500°C are listed as a function of sintering temperature, duration and composition. All density values are related to the theoretical densities given in Table 2.

From Fig. 2, especially for sintering at 1500°C, it becomes evident that the densification behaviour can be classified into three groups: the highest relative densities were achieved with the powders having low Y content (83–89%), next came powders with 16·5 at.-%Y (79–81%), and last were the powders with high Y content (73–78%). Direct correlation of Ti content with sintering behaviour was not observed. However, for all sintering temperatures powder no. 6 (high Y content, intermediate Ti content) consistently shows the lowest relative density (Fig. 2), and the influence of Ti content seems to be coupled with Y content.

The density of the bars sintered at 1500°C and measured by image analysis is often close to the value of the pellets. The results of the quantitative image analysis are listed in Tables 3 and 4. Owing to the high sintering temperature, grain coarsening and extended grain boundaries occurred, leading to the large particle diameters given in Table 4. In most cases the pore sizes are 3 to 6 times smaller than the particle sizes, indicating the formation of a well connected ceramic matrix after sintering.

Electrical conductivity

The validity of equation (1) for calculating specific conductivity was checked using the data obtained for the material with lowest Ti content, $Y_{0·165}Zr_{0·806}Ti_{0·029}O_{2-x}$. Assuming that the content of 3 at.-%Ti has no significant influence on conductivity in air,[24,25] the values determined from equation (1) should be similar to those for 8 or 9 mol-%YSZ. At 800°C, conductivities of 0·025–0·04 S cm^{-1} have been reported.[50,51] Applying equation (1) using the microstructural data listed in Table 4 and the relative density determined by image analysis (Table 3) resulted in a conductivity of 0·0318 S cm^{-1} for this compound, which is in very close agreement with the published data. Therefore calculation of specific conductivity seems to result in reliable values, and these are compiled in Table 5 together with the corresponding activation energies and the pre-exponential factors according to the formula

$$\sigma T = k \exp(-E_a/RT) \quad \ldots\ldots\ldots\ldots \quad (3)$$

Electrical conductivity in air

The dependence of electrical conductivity in air, corrected for porosity by applying equation (3), on the composition

Table 3 Densification data obtained on circular pellets fabricated from Y–Zr–Ti oxide powders after sintering for 5 h: relative final density of bars measured by quantitative image analysis

No.	Nominal composition	Sintering temp., °C	Relative initial density of pellets $\rho^{p}_{th,i}$, %	Relative final density of pellets $\rho^{p}_{th,f}$, %	Relative final density of bars $\rho^{s}_{th,f}$, %
1	$Y_{0·165}Zr_{0·735}Ti_{0·1}O_{2-x}$	1300	39·7	72·7	...
		1400	39·2	75·2	...
		1500	40·3	80·9	84·1±2·5
2	$Y_{0·11}Zr_{0·84}Ti_{0·05}O_{2-x}$	1300	40·5	82·5	...
		1400	39·9	86·1	...
		1500	40·3	89·9	75·5±2·8
3	$Y_{0·22}Zr_{0·73}Ti_{0·05}O_{2-x}$	1300	41·7	70·1	...
		1400	43·3	77·4	...
		1500	42·7	78·4	65·4±3·6
4	$Y_{0·11}Zr_{0·74}Ti_{0·15}O_{2-x}$	1300	34·9	72·5	...
		1400	35·2	79·1	...
		1500	34·7	83·0	85·7±2·3
5	$Y_{0·22}Zr_{0·63}Ti_{0·15}O_{2-x}$	1300	36·2	71·9	...
		1400	34·4	74·6	...
		1500	35·2	75·7	83·6±1·9
6	$Y_{0·243}Zr_{0·657}Ti_{0·1}O_{2-x}$	1300	43·7	65·4	...
		1400	40·0	69·7	...
		1500	44·4	72·8	71·2±2·1
7	$Y_{0·087}Zr_{0·813}Ti_{0·1}O_{2-x}$	1300	44·0	82·9	...
		1400	38·9	86·3	...
		1500	44·5	86·9	85·0±3·2
8	$Y_{0·165}Zr_{0·664}Ti_{0·171}O_{2-x}$	1300	34·2	75·7	...
		1400	33·4	76·0	...
		1500	33·6	79·9	79·6±0·9
9	$Y_{0·165}Zr_{0·806}Ti_{0·029}O_{2-x}$	1300	42·9	74·0	...
		1400	43·9	78·6	...
		1500	43·4	79·6	80·9±2·0

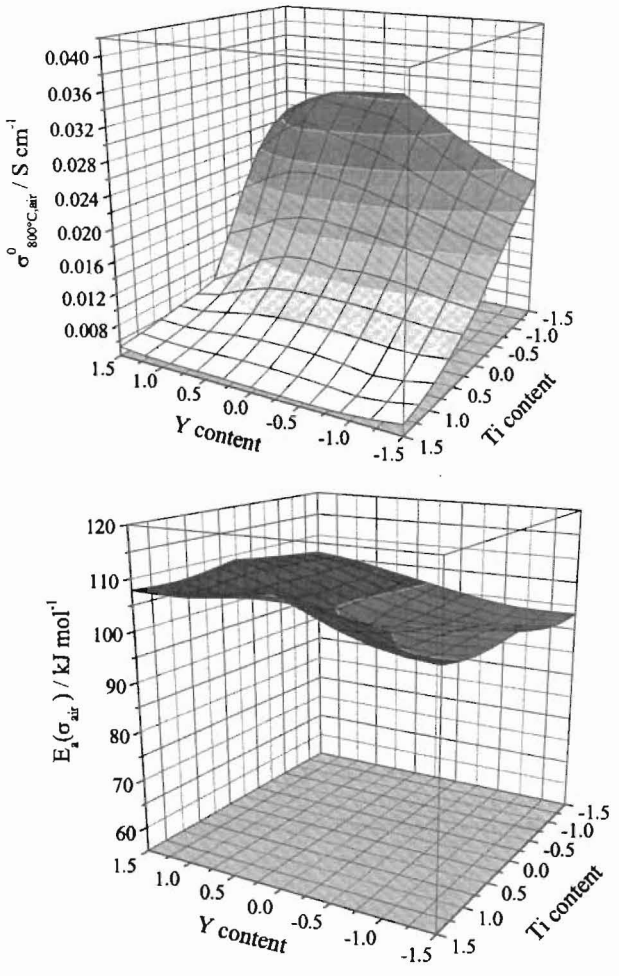

3 Electrical conductivity at 800°C measured in air after correction for porosity, and corresponding activation energies E_a: for conversion of orthogonalised Y and Ti contents x_Y and x_{Ti} into compositional concentrations *see* Table 1

of the YZT ceramics is shown in Fig. 3. The highest conductivity is achieved with the ceramic containing the lowest Ti content and 16·5 at.-%Y. At the same Ti level the conductivity decreases towards lower and higher Y contents. This is very well known from the pure Y–Zr–O system[52] owing to the decrease of oxygen vacancies and the correlation effects of vacancies, respectively.[52,53] With increasing Ti content conductivity decreases monotonically by one order of magnitude and becomes nearly independent of Y content.

The absolute values as well as the degree of decrease with increasing Ti content are in excellent agreement with previous studies.[39–41] Among the former investigations, only Colomer *et al.*[41] systematically investigated the influence of both TiO_2 and Y_2O_3 contents on conductivity in the Y–Ti–Zr–O system. In the considered compositional range for TiO_2 they also found a decrease in conductivity of one order of magnitude, and the dependence on Y_2O_3 content was more pronounced (variation in conductivity by a factor of 5) than in this investigation (factor of 2). This difference might be a result of the different experimental temperatures used: in Ref. 41 all data are presented for 500°C, whereas here conductivity was measured at 800°C, a temperature that is more relevant for SOFC operation.

The activation energies determined from the Arrhenius plots agree well with those of YSZ materials, and the slight increase in activation energy with increasing Y content was also reproduced.[52,54] In contrast, and surprisingly, the activation energies did not show any significant link with Ti content.[39,40] This means that the decrease in conductivity (in air) with increasing Ti content is due to a decrease in carrier concentration, i.e. oxygen vacancies, but not to a decrease in mobility. This in turn suggests that an increasing part of the oxygen lattice is trapped by or fixed to the Ti ions and cannot participate in the transport process, whereas the influence of decreasing lattice parameters (Table 2) with increasing Ti content does not seem to be strong.

Electrical conductivity in Ar–H_2

The results of conductivity measurements in reducing atmosphere ($p_{O_2} \approx 10^{-18}$ bar at 800°C) are summarised in Fig. 4. It is well known that under reducing conditions Ti^{3+} ions are formed and *n* type electronic conductivity is obtained.[24,25,34,36–40,42] The absolute level of the conductivity values in Fig. 4 is therefore slightly increased compared with Fig. 3. However, certain features of the plot in Fig. 4 must be emphasised. First, the samples with low Ti content are still predominantly ionic in conductivity and the local maximum conductivity is again found to be in the range 16–20 at.-%Y. Second, with increasing Ti content the total conductivity decreases until concentrations of about 10 at.-%Ti are reached. Below this Ti content the total conductivity is still strongly affected by the ionic contribution. Third, at higher Ti concentrations the conductivity becomes predominantly electronic, as can be seen from the strong increase towards the corner with high Ti and high Y concentrations. Here the maximum conductivity is about 42 mS cm^{-1}, i.e. the electronic conductivity is 10 times higher than the ionic conductivity. Fourth, most striking is the fact that such high conductivities were not obtained for similar Ti contents and low Y concentrations. This observation has not been reported before, presumably because partially stabilised zirconia materials are no longer tetragonal but form a mixture of cubic, tetragonal and monoclinic phases (Table 2). As a guide to the eye, the phase boundary between pure cubic and the originally given two phase region according to Ref. 41 is inserted in Fig. 4. When the cubic phase boundary is exceeded, electronic conductivity is strongly reduced.

As long as the ionic conductivity is the dominant contribution to the mixed conductivity in Ar–H_2, the

Table 4 Average grain size and pore size of rectangular bars used for electrical conductivity measurements

No.	Nominal composition	Average grain size, μm	Average pore size, μm
1	$Y_{0·165}Zr_{0·735}Ti_{0·1}O_{2-x}$	12·5	2·3
2	$Y_{0·11}Zr_{0·84}Ti_{0·05}O_{2-x}$	10·6	5·5
3	$Y_{0·22}Zr_{0·73}Ti_{0·05}O_{2-x}$	10·6	3·5
4	$Y_{0·11}Zr_{0·74}Ti_{0·15}O_{2-x}$	18·2	3·2
5	$Y_{0·22}Zr_{0·63}Ti_{0·15}O_{2-x}$	16·0	3·1
6	$Y_{0·243}Zr_{0·657}Ti_{0·1}O_{2-x}$	14·3	9·8
7	$Y_{0·087}Zr_{0·813}Ti_{0·1}O_{2-x}$	23·6	4·5
8	$Y_{0·165}Zr_{0·664}Ti_{0·171}O_{2-x}$	13·9	3·5
9	$Y_{0·165}Zr_{0·806}Ti_{0·029}O_{2-x}$	9·3	2·2

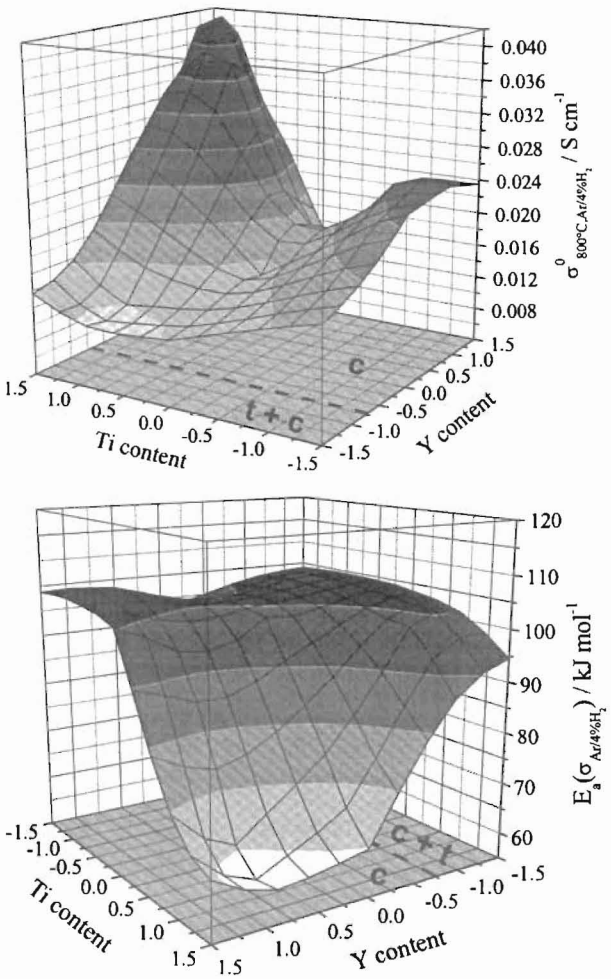

4 Electrical conductivity at 800°C measured in Ar–4%H_2 after correction for porosity, and corresponding activation energies E_a: for better presentation activation energy plot was rotated by about 180°; for conversion of orthogonalised Y and Ti contents x_Y and x_{Ti} into compositional concentrations *see* Table 1

activation energies remain in the range 90–110 kJ mol^{-1}. Only in the compositional region where high electronic conductivity was recorded did the activation energies decrease to values of around 60 kJ mol^{-1} (Table 2, Fig. 4), indicating that the apparent conduction mechanism has changed from ion to polaron hopping.[39]

STATISTICAL EVALUATION

The measured conductivity data were examined statistically using the Statgraphics Plus software package, version 4.1. In this program, the experimental parameters, i.e. x_Y and x_{Ti} in the YZT ceramics (Table 1), are termed factors A and B. For the input data sheet a multilevel factorial design was chosen rather than the classical approach for screening experiments, since the latter input version only leads to linear fits whereas the multilevel factorial evaluation also includes second order effects and coupled interactions between the experimental parameters (AA, AB, BB). In all investigated cases a 95% confidence limit was set for the mean response. Only a descriptive summary is given here for the variables investigated: the mathematical background of how to obtain diagrams is beyond the scope of the present paper and can be found in textbooks, for example Refs. 43–45.

In Fig. 5 the statistical results of the conductivity measurements in air are summarised. The upper graphs are the so called Pareto charts of the factors influencing the conductivity and activation energy data. The values shown are the effects of the individual factors divided by the standard errors. Those bars which are larger than the standard error (vertical line) have a significant impact on the determined values, as for instance Ti content on conductivity. When second order effects were considered for E_a no factor reached the level of significance and no clear dependence of any factor was found in the Pareto chart. Thus all interactions (AA, AB, BB) were omitted for further evaluation of E_a.

The plots in the middle of Fig. 5 show the main effects for the two experimental factors. On the left the dependence of conductivity on x_Y shows a slight maximum and the dependence on x_{Ti} shows a steady decrease, as already mentioned (cf. Fig. 3, top). On the right the dependence of E_a on both x_Y and x_{Ti} shows an increase with increasing amounts of Y and Ti but with a smaller slope for Ti. The image at the foot of Fig. 5 shows how the experimental parameters x_Y and x_{Ti} interact with each other. When x_Y is varied from low to high values this has a different impact on the conductivity for high and low Ti concentrations. At small x_{Ti} the conductivity increases, whereas at large x_{Ti} the conductivity decreases slightly.

The equations fitting the model to the conductivity and corresponding E_a values are

$$\sigma_{800,air} = 1{\cdot}26\times10^{-2} + 4{\cdot}99\times10^{-4}x_Y - 9{\cdot}89\times10^{-3}x_{Ti} - 1{\cdot}51\times10^{-3}x_{Y^2} - 2{\cdot}33\times10^{-3}x_Y x_{Ti} + 3{\cdot}34\times10^{-3}x_{Ti^2} \quad (4)$$

and

$$E_a(\sigma_{800,air}) = 103{\cdot}25 + 3{\cdot}20x_Y + 2{\cdot}18x_{Ti} \quad (5)$$

The R^2 statistic indicates that the model as fitted explains 95·2 and 60·2% of the variability in $\sigma_{800,air}$ and $E_a(\sigma_{800,air})$, respectively.

Statistical assessment of the conductivities measured in Ar–H_2 and of the resulting activation energies reveals that the standardised effect of the coupled factor AA was <0·01 and can therefore be neglected. Nevertheless, in the case of the conductivity values all the factors were found to be below the level of significant impact (see lefthand Pareto chart in Fig. 6). This means that the model (or equation) used cannot reproduce the complex isothermal shape shown in Fig. 4. This is not surprising since the model takes into account only quadratic terms in the equation, but the profile in Fig. 4 is more complicated and certainly contains at least cubic terms. As a consequence, the plots of the main effects and interactions between the variables (Fig. 6, left) give only simple and tentative dependences, and the equation fitted to the conductivity in reducing atmosphere

$$\sigma_{800,Ar-H_2} = 1{\cdot}32\times10^{-2} + 4{\cdot}54\times10^{-3}x_Y + 1{\cdot}38\times10^{-3}x_{Ti} + 5{\cdot}48\times10^{-3}x_Y x_{Ti} + 7{\cdot}40\times10^{-3}x_{Ti^2} \quad (6)$$

is not a good approximation of the measured conductivities, a fact which is also indicated by the low R^2 value of 61·9%.

In contrast the determined activation energies can be fitted very well, since the Ti content and also the coupled terms BB and AB, i.e. all terms in which x_{Ti} is involved, are of considerable significance (see righthand Pareto chart in Fig. 6). The influence of the experimental parameters is well described by the model (small and strong decrease in E_a with increasing x_Y and x_{Ti}, respectively). The plot of interactions (Fig. 6, bottom) explains why at low x_{Ti} the value of E_a is not changed (Fig. 4): here the interaction between x_Y and x_{Ti} is positive and compensates the

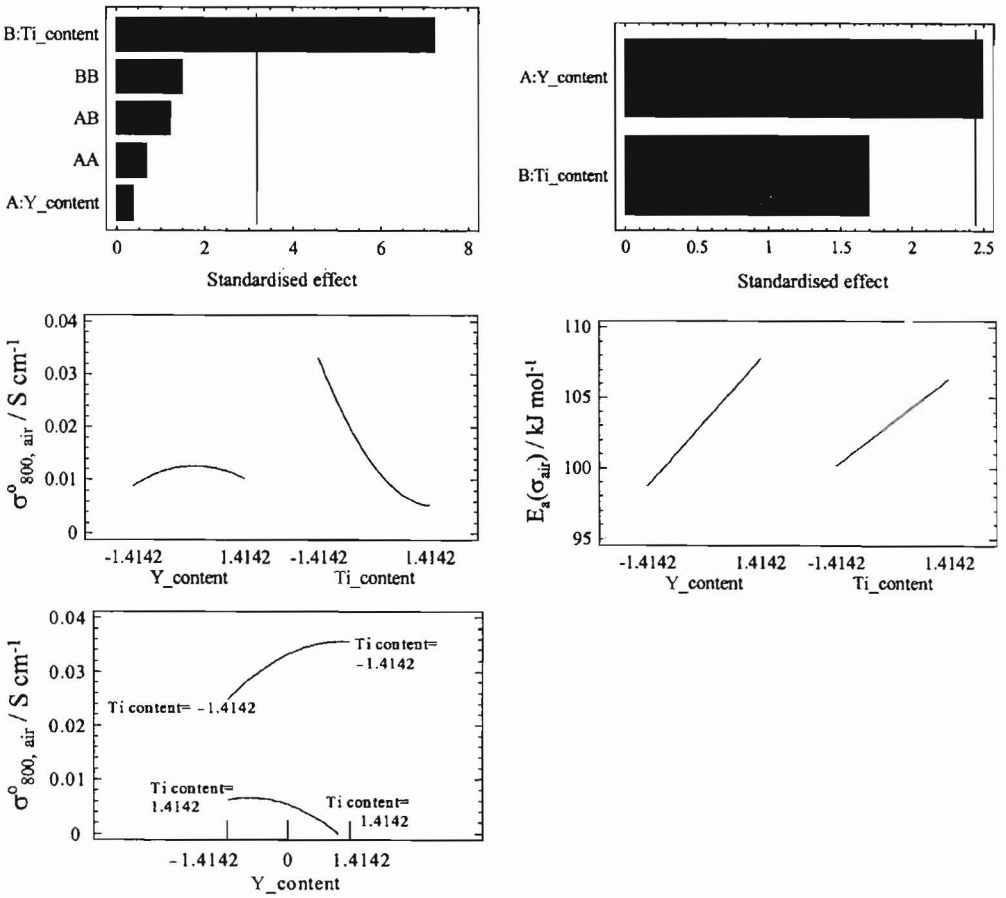

5 Standardised Pareto chart (top), plot showing main trends in experimental factors (middle) and plot showing interaction between experimental factors (bottom) for conductivity measured in air at 800°C (left) and corresponding activation energies (right)

negative trend for the pure dependence on x_Y. At high x_{Ti}, however, the interaction between x_Y and x_{Ti} supports the pure decreasing dependence of E_a on x_{Ti}. The E_a values are fitted well by the equation

$$E_a(\sigma_{800,Ar-H_2}) = 103{\cdot}31 - 5{\cdot}33x_Y - 12{\cdot}30x_{Ti} - 11{\cdot}41x_Y x_{Ti} - 11{\cdot}14x_{Ti^2} \quad (7)$$

and the R^2 statistic indicates that the model was able to fit 91·6% of the variability in $E_a(\sigma_{800,Ar-H2})$.

In summary, the statistical design of experiments for compositional optimisation and the statistical assessment of the results can give more insight into the observed dependences, especially when more than two parameters are changed and when coupled effects become important (as shown here for $E_a(\sigma_{800,Ar-H_2})$). As long as the variable changes without an inflection point, the models can fit the experimental data very well. However, the computer based statistical analysis reaches its limits as soon as complex dependences are obtained experimentally, as here for the conductivity values shown in Fig. 4. The available models and equations are then either too simple or require more experimental data.

For a technological approach to materials selection, the statistical design of experiments can give a rapid overview of the materials properties in the chosen compositional region. This has been clearly demonstrated for electrical conductivity in air, for which a similar three-dimensional shape was reproduced to that produced by Colomer *et al.*[41] The difference between the two investigations is that in the present case only nine different compositions were investigated instead of 43 samples.

APPLICABILITY OF YZT CERAMICS IN SOFCS

To improve the electrochemical performance of SOFC anodes, it is necessary to combine materials with the highest ionic and electronic conductivity. Thus the state of the art anode material is a composite of YSZ and Ni metal. A mixed conducting ceramic certainly will not have an electronic conductivity like Ni, but it should show at least 50–100 S cm^{-1} at SOFC operating conditions to avoid high ohmic losses. Such conductivity values are difficult to achieve with *n* type materials but some examples can be found.[34,35] The more critical parameter is the ionic conductivity, which should remain at a high level as known for solid oxide electrolytes.

In the present study, however, the electronic conductivity of the YZT ceramics is too low to substitute for metallic Ni. Additionally, the ionic conductivity decreases with increasing electronic conductivity. This means that the slowest conduction path in the SOFC becomes even slower. This has been demonstrated very recently by testing an SOFC with Ni/YZT anode.[55] The comparison with a conventional SOFC shows that the power density is much lower for the cell with Ni/YZT anode. Therefore YZT ceramics seem to be promising materials for SOFCs only when the Ti content is low.

CONCLUSIONS

Oxides of Y–Zr–Ti can be conveniently synthesised by the coprecipitation technique. The densification behaviour of the powders depends very much on the Y content but not on the Ti content. The conductivities and activation energies measured in air agree very well with previous

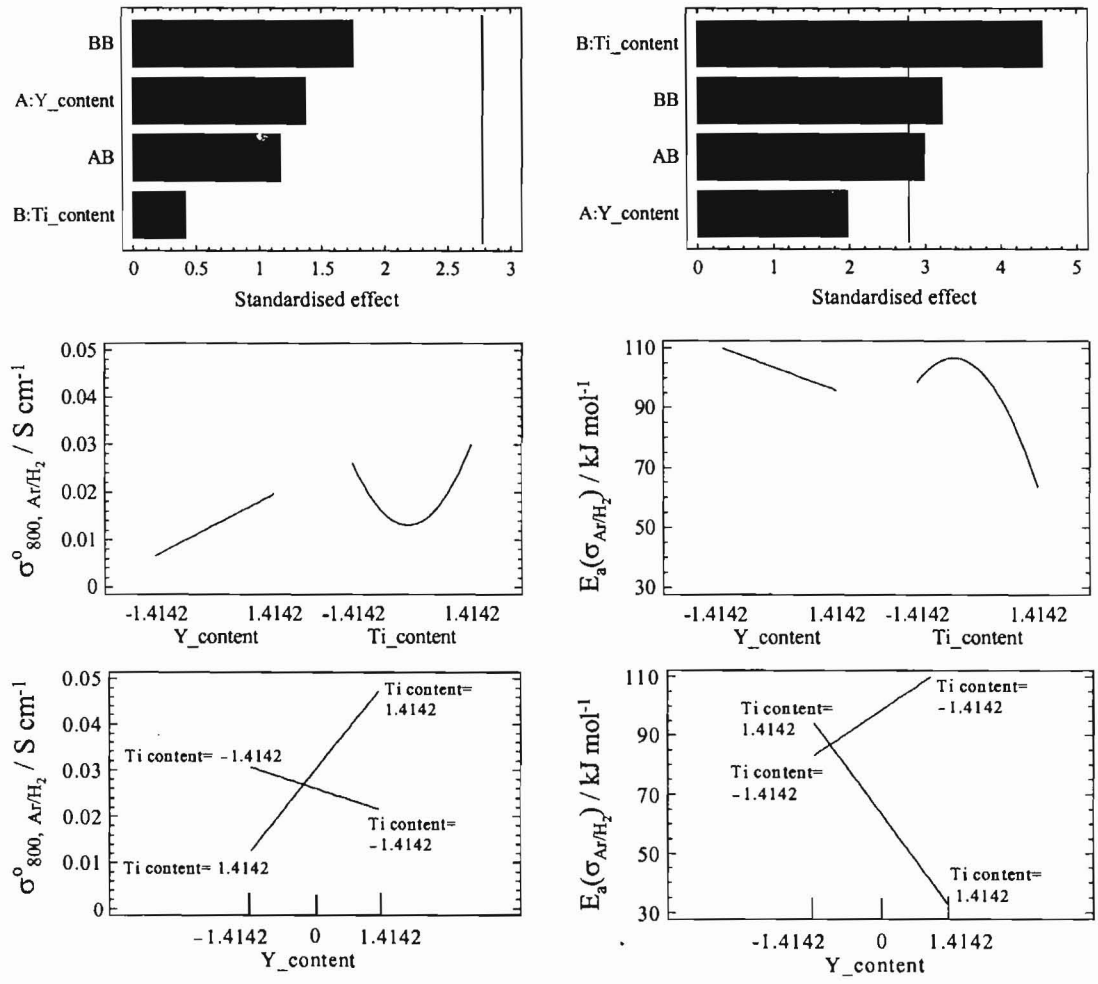

6 Standardised Pareto chart (top), plot showing main trends in experimental factors (middle) and plot showing interaction between experimental factors (bottom) for conductivity measured in Ar–4%H_2 at 800°C (left) and corresponding activation energies (right)

Table 5 Electrical dc conductivity of YZT oxides measured in air and Ar–4%H_2, corresponding activation energies E_a between 500 and 900°C and pre-exponential factors k

No.	Nominal composition	Temp., °C	σ in air, mS cm^{-1}	σ in Ar–4%H_2, mS cm^{-1}	$E_{a,air}$, kJ mol^{-1}	log$k_{,air}$ (S cm^{-1} K^{-1})	$E_{a,Ar-H_2}$, kJ mol^{-1}	log$k_{,Ar-H_2}$ (S cm^{-1} K^{-1})
1	$Y_{0.165}Zr_{0.735}Ti_{0.1}O_{2-x}$	900	30·3	33·4	98·2±0·9	5·90±0·05	100·5±1·1	6·05±0·06
		800	12·6	14·0				
		700	4·4	4·6				
2	$Y_{0.11}Zr_{0.84}Ti_{0.05}O_{2-x}$	900	46·2	37·2	96·6±0·8	6·05±0·04	104·2±2·1	6·32±0·11
		800	20·2	16·1				
		700	7·3	5·8				
3	$Y_{0.22}Zr_{0.73}Ti_{0.05}O_{2-x}$	900	71·5	62·4	106·0±0·8	6·66±0·04	105·8±1·6	6·59±0·08
		800	30·6	26·2				
		700	9·9	8·7				
4	$Y_{0.11}Zr_{0.74}Ti_{0.15}O_{2-x}$	900	12·1	23·5	100·0±1·7	5·97±0·08	102·7±2·3	6·02±0·11
		800	4·8	9·8				
		700	1·8	3·2				
5	$Y_{0.22}Zr_{0.63}Ti_{0.15}O_{2-x}$	900	14·7	76·7	105·5±2·2	5·91±0·11	58·7±0·9	4·46±0·06
		800	5·5	41·6				
		700	1·7	20·9				
6	$Y_{0.243}Zr_{0.657}Ti_{0.1}O_{2-x}$	900	15·9	19·9	109·1±1·2	6·13±0·06	104·0±0·9	5·99±0·05
		800	6·3	8·1				
		700	2·0	2·7				
7	$Y_{0.087}Zr_{0.813}Ti_{0.1}O_{2-x}$	900	24·6	26·6	101·6±1·0	6·00±0·05	104·1±0·8	6·15±0·04
		800	10·5	11·1				
		700	3·6	3·6				
8	$Y_{0.165}Zr_{0.664}Ti_{0.171}O_{2-x}$	900	13·4	53·3	111·3±2·5	5·66±0·20	62·8±2·8	4·47±0·16
		800	4·8	25·8				
		700	1·5	11·9				
9	$Y_{0.165}Zr_{0.806}Ti_{0.029}O_{2-x}$	900	70·0	58·0	100·9±1·2	6·43±0·07	97·9±1·0	6·18±0·05
		800	31·8	24·3				
		700	11·0	8·8				

studies carried out on single series of solid solutions. The higher conductivities measured in $Ar–H_2$ reflect the mixed conductivity of the materials. High electronic contributions were detected for materials with $c_{Ti} \geq 0{\cdot}15$ and $c_Y \geq 0{\cdot}2$, whereas a smaller Y content leads to a decrease in conductivity and the formation of three zirconia phases.

The statistical assessment and fitting of the experimental data revealed good agreement with the conductivity measurements in air. For the conductivity measurements in reducing atmosphere the fitting was limited owing to the complex dependence of the experimental data. Instead, the corresponding activation energies were analysed satisfactorily and the values obtained from the measurements in $Ar–H_2$ yielded a significant coupled influence of both compositional parameters.

Statistical design of experiments is a very useful tool for rapid materials selection, and even more complex systems may be statistically analysed than those discussed here.

ACKNOWLEDGEMENTS

The authors thank colleagues at FZJ for their experimental help with this work, especially Mr P. Lersch (FZJ-IWV2) for the XRD measurements, Dr W. Fischer (FZJ-IWV2) for the Rietveld analyses, Mr M. Michulitz (FZJ-ZCH) for the ICP–OES measurements and Mrs Gutzeit (FZJ-IWV2) for the microstructural image analysis. Helpful discussions with Dr Glüsen (FZJ-IWV3) on the statistical assessment are greatly appreciated. Financial support from CSIR, New Delhi and BMBF, Berlin/Bonn for this joint research work under the Indo-German bilateral cooperation project (grant INI-041-99) is gratefully acknowledged.

REFERENCES

1. L.-W. TAI, M. M. NASRALLAH, H. U. ANDERSON, D. M. SPARLIN and S. R. SEHLIN: *Solid State Ionics*, 1995, **76**, 259.
2. W. J. QUADAKKERS, H. GREINER, M. HÄNSEL, A. PATTANAIK, A. S. KHANNA and W. MALLÉNER: *Solid State Ionics*, 1996, **91**, 55.
3. T. ISHIHARA, H. MATSUDA and Y. TAKITA: *J. Am. Chem. Soc.*, 1994, **116**, 3801.
4. M. FENG and J. B. GOODENOUGH: *Eur. J. Solid State Chem.*, 1994, **31**, 663.
5. R. KOE and H. U.ANDERSON: *J. Mater. Sci.*, 1992, **27**, 5837.
6. B. C. H. STEELE: *Solid State Ionics*, 1996, **86–88**, 1223.
7. S. T. ARUNA, M. MUTHURAMAN and K. C. PATIL: *J. Mater. Chem.*, 1997, **7**, 2499.
8. S. T. ARUNA, M. MUTHURAMAN and K. C. PATIL: *Solid State Ionics*, 1998, **111**, 45.
9. H. S. MAITI, A. CHAKRABORTHY and M. K. PARIA: Proc. 3rd Int. Symp. on Solid Oxide Fuel Cells, 190; 1993, Pennington, NJ, Electrochemical Society.
10. R. DOSHI, V. L. RICHARDS, J. D. CHARTER, X. WANG and M. KRUMPELT: *J. Electrochem. Soc.*, 1999, **146**, 1273.
11. A. PETRIC, P. HUANG and F. TIETZ: *Solid State Ionics*, 2000, **135**, 719.
12. W. BAKKER, K. HUANG, J. B. GOODENOUGH, A. KHANDKAR and S. ELANGOVAN: Abstracts of the Fuel Cell Seminar, Palm Springs, CA, USA, November 1998, 250.
13. P. HUANG and A. PETRIC: *J. Electrochem. Soc.*, 1996, **143**, 1644.
14. T. ISHIHARA, M. HONDA, T. SHIBAYAMA, H. MINAMI, H. NISHIGUCHI and Y. TAKITA: *J. Electrochem. Soc.*, 1998, **145**, 3177.
15. A. AHMAD-KHANLOU, F. TIETZ, I. C. VINKE and D. STÖVER: Proc. 7th Int. Symp. on Solid Oxide Fuel Cells (SOFC-VII), 476; 2001, Pennington, NJ, Electrochemical Society.
16. T. TSAI and A. BARNETT: Proc. 5th Int. Symp. on Solid Oxide Fuel Cells (SOFC-V), 369; 1997, Pennington, NJ, Electrochemical Society.
17. G . STOCHNIOL, H. GRUEBMEIER, A. NAOUMIDIS and H. NICKEL: Proc. 4th Int. Symp. on Solid Oxide Fuel Cells (SOFC-IV), 995; 1995, Pennington, NJ, Electrochemical Society.
18. F. TIETZ, I. ARUL RAJ, W. JUNGEN and D.STÖVER: *Acta Mater.*, 2001, **49**, 803.
19. I. ARUL RAJ, F. TIETZ, A. GUPTA, W. JUNGEN and D. STOVER: *Acta Mater.*, 2001, **49**, 1987.
20. R. N. BASU, F. TIETZ, O. TELLER, E. WESSEL, H. P. BUCHKREMER and D. STÖVER: *J. Solid State Electrochem.*, 2003, **7**, 416.
21. R. MARIC, S. OHARA, T. FUKUI, T. INAGAKI and J. FUJITA: *Electrochem.: Solid State Lett.*, 1998, **1**, 201.
22. P. COSTAMAGNA, P. COSTA and E. ARATO: *Electrochim. Acta*, 1998, **43**, 967.
23. M. MORI, T. YAMAMOTO, H. ITOH, H. INABA and H. TAGAWA: *J. Electrochem. Soc.*, 1998, **145**, 1374.
24. S. S. LIOU and W. L. WORRELL: *Appl. Phys. A*, 1989, **49**, 25.
25. K. E. SWIDER and W. L. WORRELL: *J. Electrochem. Soc.*, 1996, **143**, 3706.
26. K. KOBAYASHI, Y. KAI, S. YAMAGUCHI, N. FUKATSU, T. KAWASHIMA and Y. IGUCHI: *Solid State Ionics*, 1997, **93**, 193.
27. K. KOBAYASHI, S. YAMAGUCHI, T. HIGUCHI, S. SHIN and Y. IGUCHI: *Solid State Ionics*, 2000, **135**, 643.
28. T. HORITA, N. SAKAI, T. KAWADA, H. YOKOKAWA and M. DOKIYA: *J. Electrochem. Soc.*, 1996, **143**, 1161.
29. A. L. DICKS: *J. Power Sources*, 1996, **61**, 113.
30. A. KELAIDOPOULOU, A. SIDDLE, A. L. DICKS, A. KAISER and J. T. S. IRVINE: *Fuel Cells*, 2001, **1**, 226.
31. C. M. REICH, A. KAISER and J. T. S. IRVINE: *Fuel Cells*, 2001, **1**, 249.
32. M. GONZÁLEZ-CUENCA, W. ZIPPRICH, B. A. BOUKAMP, G. PUDMICH and F. TIETZ: *Fuel Cells*, 2001, **1**, 256.
33. O. A. MARINA and L. R. PEDERSON: Proc. 5th Eur. SOFC Forum, Lucerne, Switzerland, June 2002, Vol. 1, 481.
34. R. MOOS and K. H. HÄRDTL: *J. Appl. Phys.*, 1996, **80**, 393.
35. G. PUDMICH, B. A. BOUKAMP, M. GONZALEZ-CUENZA, W. JUNGEN, W. ZIPPRICH and F. TIETZ: *Solid State Ionics*, 2000, **135**, 433.
36. F. TIETZ, W. JUNGEN, P. LERSCH, M. FIGAJ, K. D. BECKER and D. SKARMOUTSOS: *Chem. Mater.*, 2002, **14**, 2252.
37. S. S. LIOU and W. L. WORRELL: Proc. 1st Int. Symp. on SOFCs, 81; 1989, Pennington, NJ, Electrochemical Society.
38. A. KAISER, A. J. FEIGHERY, D. P. FAGG and J. T. S. IRVINE: *Ionics*, 1998, **4**, 215.
39. H. NAITO and H. ARASHI: *Solid State Ionics*, 1992, **53–56**, 436.
40. M. T. COLOMER, J. R. JURADO, R. M. C. MARQUES and F. M. B. MARQUES: Proc. 2nd Int. Symp. on Ionic and Mixed Conducting Ceramics, 369; 1994, Pennington, NJ, Electrochemical Society.
41. M. T. COLOMER, P. DURÁN, A. CABALLERO and J. R. JURADO: *Mater. Sci. Eng. A*, 1997, **229**, 114.
42. A. J. FEIGHERY, J. T. S. IRVINE, D. P. FAGG and A. KAISER: *J. Solid State Chem.*, 1999, **143**, 273.
43. V. ANDERSON and R. MCLEAN: 'Design of experiments', 1st edn; 1974, New York, NY, Marcel Dekker.
44. G. BOX, W. HUNTER and J. HUNTER: 'Statistics for experiments'; 1979, New York, NY, Wiley.
45. B. GIMPEL: 'Qualitätsgerechte Optimierung von Fertigungsprozessen'; 1991, Dusseldorf, VDI-Verlag.
46. A. R. BOCCACCINI and Z. FAN: *J. Am. Ceram. Soc.*, 1996, **79**, 2997.
47. Z. FAN, A. P. MIODOWNIK and P. TSAKIROPOULOS: *Mater. Sci. Technol.*, 1993, **9**, 1094.
48. D. SIMWONIS, F. TIETZ and D. STÖVER: *Solid State Ionics*, 2000, **132**, 241.
49. H. YOKOKAWA, N. SAKAI, T. KAWADA and M. DOKIYA: Proc. Science and Technology of Zirconia V, 59; 1993, Lancaster, PA, Technomic.
50. J. VAN HERLE, A. J. MCEVOY and K. RAVINDRANATHAN THAMPI: *J. Mater. Sci.*, 1994, **29**, 3691.
51. F. T. CIACCHI, K. M. CRANE and S. P. S. BADWAL: *Solid State Ionics*, 1994, **73**, 49.
52. A. I. IOFFE, D. S. RUTMAN and S. V. KARPACHOV: *Electrochim. Acta*, 1978, **23**, 141.
53. H. SCHMALZRIED: *Z. Phys. Chem. Neue Folge*, 1977, **105**, 47.
54. A. P. SELLARS and B. C. H. STEELE: Proc. 2nd Eur. Ceramic Society Conf. (ECerS '91), Vol. 3, 2091; 1991, Cologne, Deutsche Keramische Gesellschaft.
55. D. SKARMOUTSOS, P. NIKOLOPOULOS, F. TIETZ and I. C. VINKE: *Solid State Ionics*, 2004, **170**, 153–158.